Supplementary Information

A facile synthesis of multi metal-doped ZnO rectangular nanocrystals using a nanocrystalline metal-organic framework template

Dong Ki Lee,[a] Jung Hyo Park,[a] Ji Il Choi,[b] Yeob Lee,[a] Sang Jun Kim,[a] Gyu-Heon Lee,[a] Yong-Hoon Kim,[b] and Jeung Ku Kang [a,b,*]*

[a] Department of Materials Science & Engineering, [b] Graduate School of Energy, Environment, Water, and Sustainability (EEWS), Korea Advanced Institute of Science and Technology (KAIST), 291 Daehak-ro, Yuseong-gu, Daejon 305-701, Republic of Korea,

Tel: +82-42-350-1780, Fax: +82-42-350-3310

E-mail: jeung@kaist.ac.kr and y.h.kim@kaist.ac.kr

Contents

Section 1. Experimental section

All reagents were used without further purification. Terephthalic acid, zinc nitrate hexahydrate, zinc acetate dehydrate, iron acetylacetonate, cobalt acetylacetonate, nickel acetylacetonate, copper acetylacetonate and *N,N*-dimethylformamide (DMF) were purchased from Aldrich. *N,N*-diethylformamide (DEF), chloroform and acetone were purchased from Tokyo Chemical Industry, Merck and Duksan Hichem, respectively.

Preparation of nanocrystalline MOF-5 (n-MOF-5): Fresh DMF stock solutions of 5 mL of zinc acetate dehydrate (7.74 mmol) and 4 mL of terephthalic acid (3.05 mmol) were added in a 20 mL vial, and then powder precipitates formed immediately upon mixing. The vial was sealed and placed in a microwave oven (700 W) and allowed to react for 10 sec. The nanocrystals were washed three times with DMF and acetone, and then immersed in acetone for 3 days. Finally, it was vacuum-dried at room temperature for 1day.

Insertion of metal ions and calcination: The metal ion saturated solutions were prepared with metal acetylacetonates ($M(acac)_2$) and 20 mL of chloroform for MOF-5s and acetone for n-MOF-5s, and detail concentrations of $M(acac)_2$ are listed in Table S1. The pore activated MOF-5 and n-MOF-5 was immersed in the each solution for 3 days, and then vacuum-dried at room temperature for 1 day. Finally, they were transferred to the box furnace and calcined at 525°C for 2 hours in air at a heating and cooling rate of 1°C min^{-1}.

Characterizations: Powder X-ray data were collected using RIGAKU SmartLab θ-2θ diffractometer in reflectance Bragg-Brentano geometry employing Johansson type Ge(111) monochromator filtered Cu Kα1 radiation at 1200W (40 KV, 30 mA) power and equipped with high speed 1D detector (D/teX Ultra). The scanning rate was 2° min^{-1} with an angular resolution of 0.01°. Gas adsorption analysis was performed on a Quantachrome Autosorb-1 automatic

volumetric instrument. A liquid nitrogen bath (77 K) and ultra-high purity grade nitrogen and helium were used for nitrogen adsorption experiment. For measurement of the apparent surface areas, the BET method was applied using the adsorption branches of the N_2 isotherms assuming a N_2 cross-sectional area of 16.2 $Å^2$/molecule. The microscopic images were observed by JEOL JEM-ARM200F Cs-corrected scanning transmission electron microcopy (STEM) and JEOL JSM-7401F scanning electron microscopy (SEM). The electron energy loss spectroscopy (EELS) spectrum was collected with GATAN Quantum SE. The energy dispersive X-ray spectrometer (EDS) images were observed by using a BRUKER QUANTAX EDS (Figs. S1 – S4). The X-ray/ultraviolet photoelectron spectroscopy (XPS and UPS) measurement was carried out a THERMO SCIENTIFIC Sigma Probe with photon source of the monochromatized Al Kα and UV source of He I (21.2 eV). The diffused reflectance spectra were determined by a VARIAN Cary-300 UV-Vis spectrophotometer with DRA-CA-30I. The magnetic properties were measured using a MicroSense EV9 vibrating sample magnetometer (VSM) at room temperature.

Synthesis and characterization of ZnO:M based on bulk MOF-5: Zinc nitrate tetrahydrate (1.20 mmol) and terephthalic acid (0.50 mmol) were first dissolved in DEF (5 mL) in a 20 mL vial. The tightly sealed vial was placed in an oven at 110 °C for 20 hours to yield clear crystals of about 1 to 2 mm in size. After cooling to room temperature, the crystals were washed with DMF three times. The product was then immersed in chloroform for 3 days to exchange solvent, and vacuum-dried at room temperature for 1 day. Insertion of metal ions to the bulk MOF-5 and calcination were proceeded as in the case of n-MOF-5, from which we obtained metal doped ZnO of about 100 to 200 nm in size. Characterization data of these ZnO nanocrystals are presented in Fig. S5.

Table S1. The concentraions of the metal ion saturated chloroform and acetone solutions.

	$Fe(acac)_2$ (mol)	**$Co(acac)_2$** (mol)	**$Ni(acac)_2$** (mol)
MOF-5:Fe	0.4		
MOF-5:FeCo	0.3	0.1	
MOF-5:FeCoNi	0.2	0.1	0.1

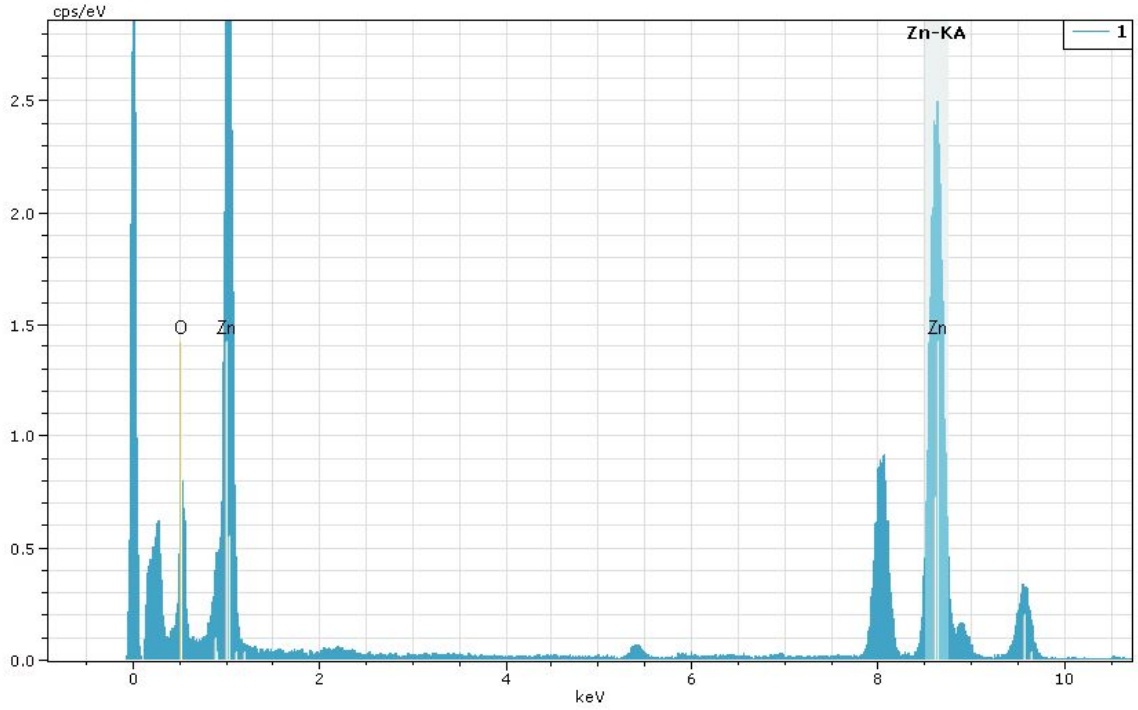

Fig. S1 EDS elecment data of r-ZnO

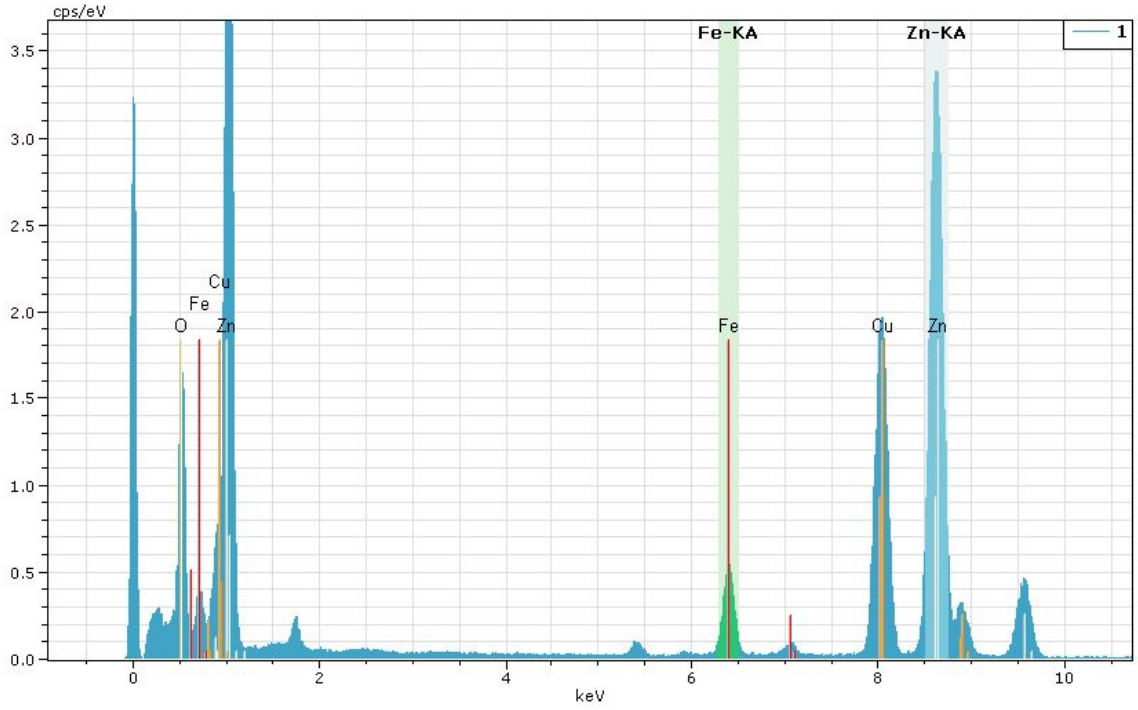

Fig. S2 EDS elecment data of r-ZnO:Fe

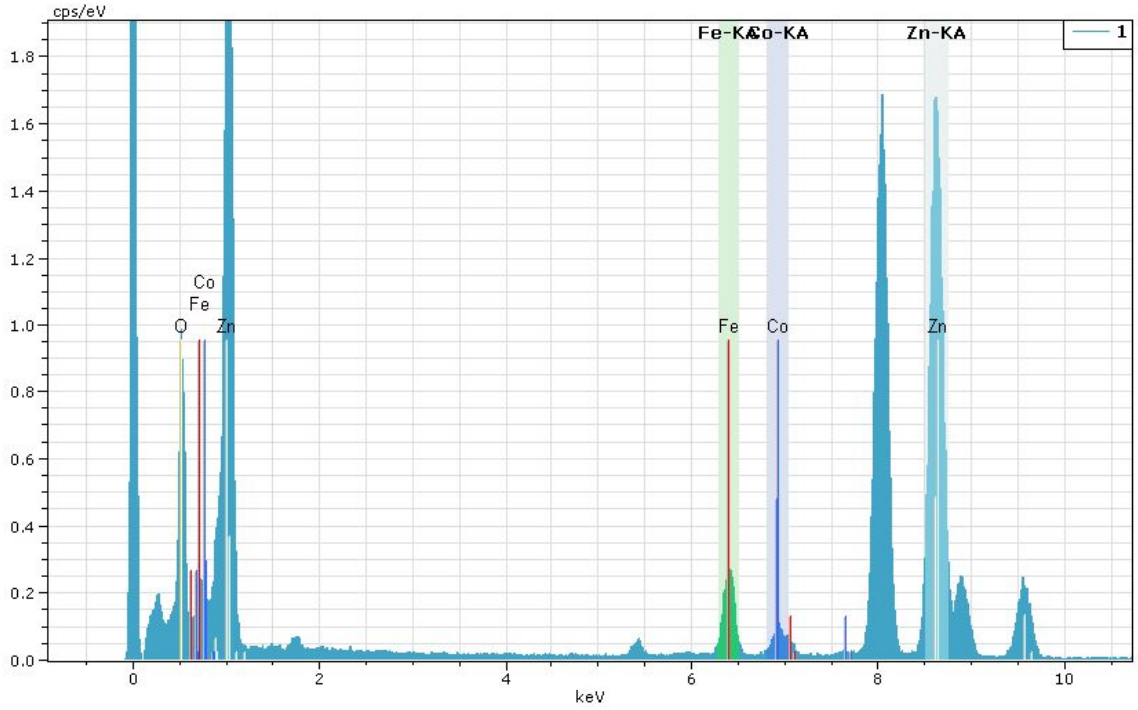

Fig. S3 EDS data of r-ZnO:FeCo

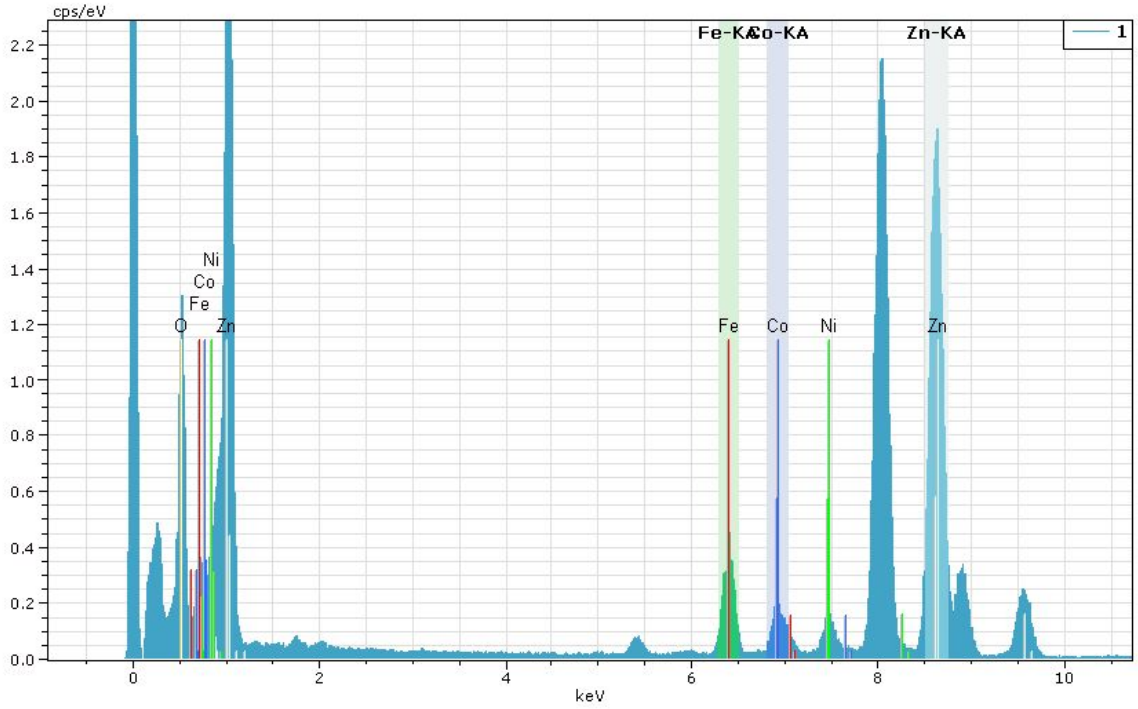

Fig. S4 EDS elecment data of r-ZnO:FeCoNi

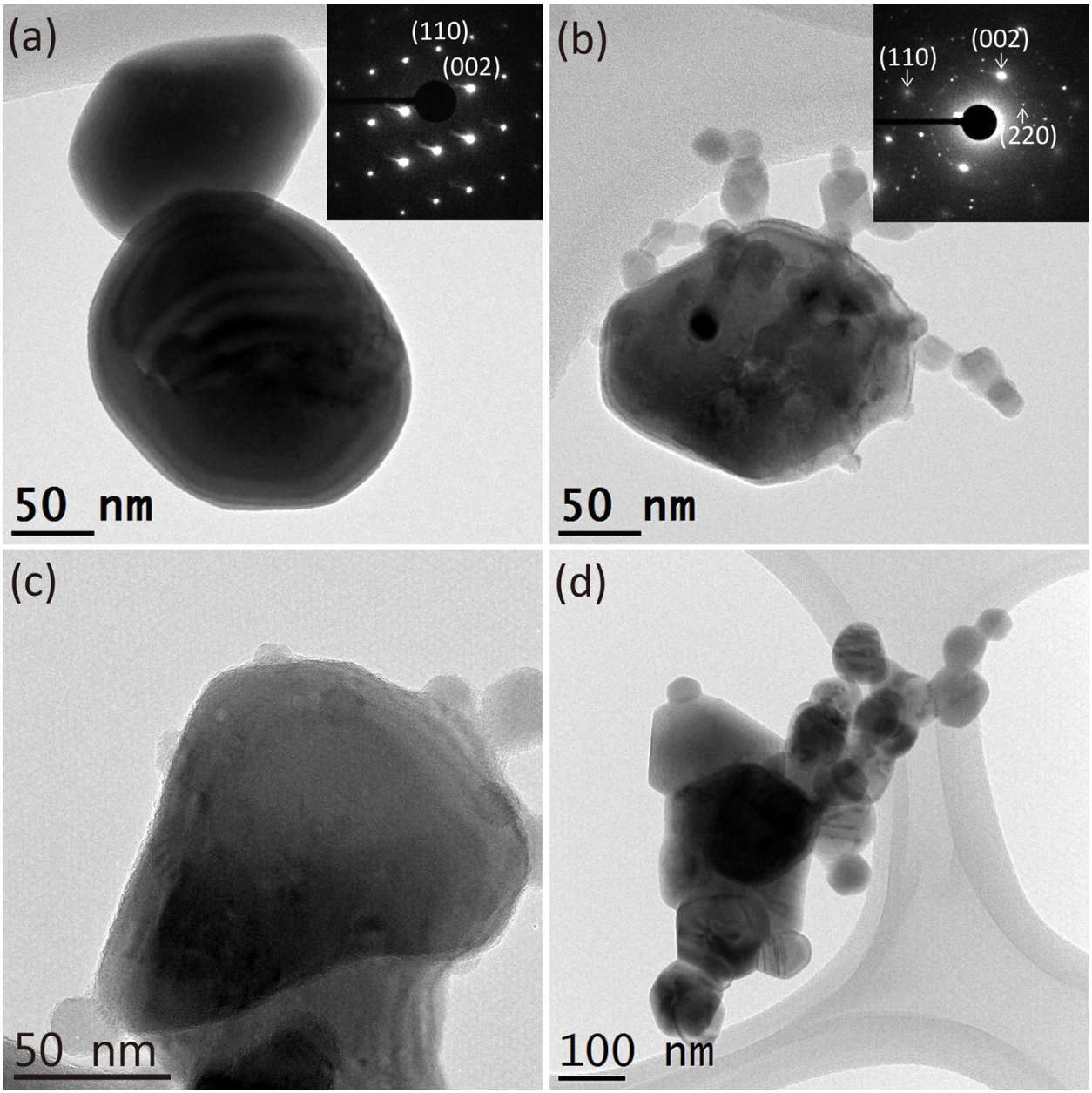

Fig. S5 TEM images of un-doped and M-doped ZnO nanocrystals synthesized using the bulk MOF-5 as a template. (a) ZnO (b) ZnO:Fe (c) ZnO:FeCo (d) ZnO:FeCoNi. The selected area electron diffraction (SAED) patterns in inset of (a) and (b) shows nanoparticles have wurtzite crystal structure. The weak (220) reflection in a inset of (b) indicates that a small amount of cubic phase is also presented in the ZnO:Fe nanoparticles.

Section 2. Computational section

A. Computational Details

Density functional theory (DFT) calculations were performed using the Vienna Ab-initio Simulation Package (VASP) [1-3] within the DFT+U scheme, in which the on-site interaction correction by Dudarev *et al*. [4] is introduced to the Perdew-Burke-Ernzerholf parameterization of the generalized gradient approximation (GGA) [5] to resolve the incorrect over-binding of electrons for the ZnO and FeO within the pure GGA or local density approximation [6, 7]. The U-J parameters applied to Zn 3d and/or Fe tune the positions of their 3d bands to the experimental values and avoid the incorrect strong correlation between the 3d orbitals and oxygen 2p orbitals. Based on the energy position of 3d orbitals from experiments [8], we used U-J = 7.0 eV for Zn (3d), 5.0 eV for the Fe (3d), and 6.1 eV for Co (3d) and Ni (3d). In good agreement with other reports [9-11], these parameters produced the band gaps of 1.56eV for the ZnO and 1.2 eV for the FeO rocksalt phase. The plane-wave energy cutoff of 400 eV was adopted. The atomic structures were fully optimized until the forces were converged to less than 0.01 eV/Å, while the redefined supercell lattice parameters were fixed as the ratio of reported unit cell values of ZnO, a = b = 3.249 Å, c = 5.205 Å, $\alpha = \beta = 90°$, and $\gamma = 120°$. To match the experimental situations [12, 13], we assigned the initial magnetic moments in the ferromagnetic configuration. Density of states were calculated with the Gaussian smearing of 0.1 eV.

B. Fe-doped ZnO Structures

To accommodate the maximum iron doping ratio up to 14.60%, we used an orthorhombic supercell structure composed of 96 atoms derived from a 4×3×2 wurtzite supercell. Brillouin zone was sampled at the 2×2×2 k-point mesh within the Monkhorst-Pack scheme. Fe-doped ZnO doped structures show well-defined wurtzite structures within the evaluated doping ratios. In geometries, energy minimized FeO and ZnO structures show small difference in bonds and angles. Fe ~ O bonds show slightly increased due to the longer bond length of FeO (2.166 Å) in bulk FeO rock salt structure, and it results in a slightly smaller angle of O-Fe-O compared to that of O-Zn-O in bulk ZnO wurtzite structure. Comparing the XRD patterns from simulations (Fig. S1) with the experiment data (Fig. 1c) shows the well-matched peak positions. It implies that the simulation models faithfully represent the experimentally observed FeO doped ZnO wurtzite structures.

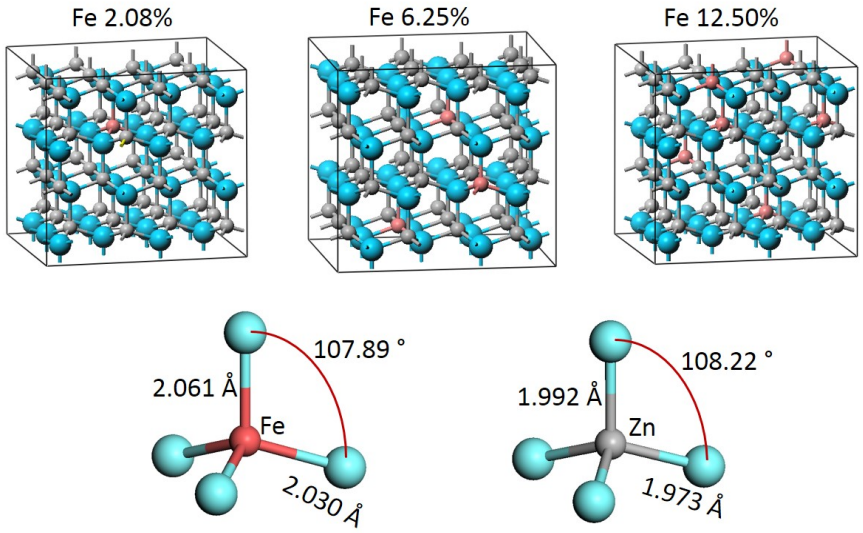

Fig. S6 FeO-doped ZnO supecells at each conenctration and geometry of energy minimized FeO-doped and un-doped ZnO. It shows the captured bond connections with nearest neighboring oxygen atoms.

C. $ZnFe_2O_4$ Spinel Structures

Normal-, and inverse-spinel structure formation depends on experimental conditions. The normal spinel structure was simulated with 56 atoms, eight Zn atoms at tetrahedral sites, 16 Fe atoms at octahedral sites, and 32 oxygen atoms [Fig. S7(a)], while the eight tetrahedral sites at the inverse spinel structure were replaced by Fe atoms [Fig. S7(b)]. Lattice parameters were determined from the JCPDS and kept constant during calculations, $a = b = c = 8.441$ Å.

Figure S8 shows the calculated XRD patterns of the normal spinel structure compared with those of the ZnO wurtzite structure. The XRD pattern matches well with the known ZnO spinel structure in JCPDS card (No. 01-070-6491).

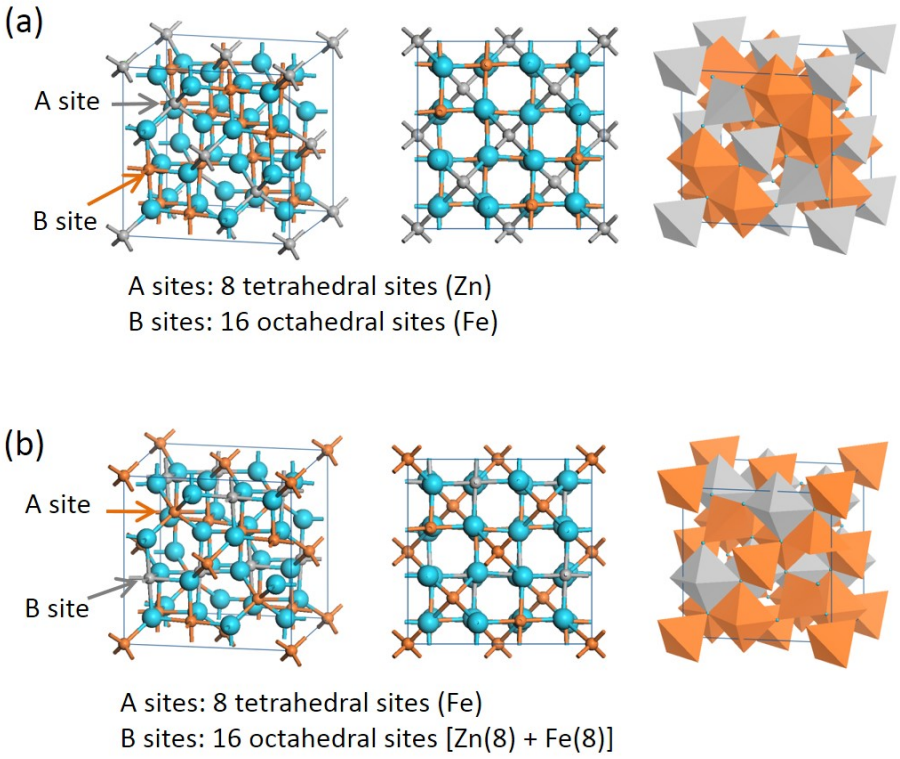

Fig. S7 (a) nomal spinel and (b) full inverse spinel strucutred $ZnFe_2O_4$ supercells. From the full inverse structure, Fe atoms occupy eight eterahedral sites. Each site, tetrahedral and octahedral sites are illusrated at each figures with differenct colors, Zn(Gray) and Fe(Orange).

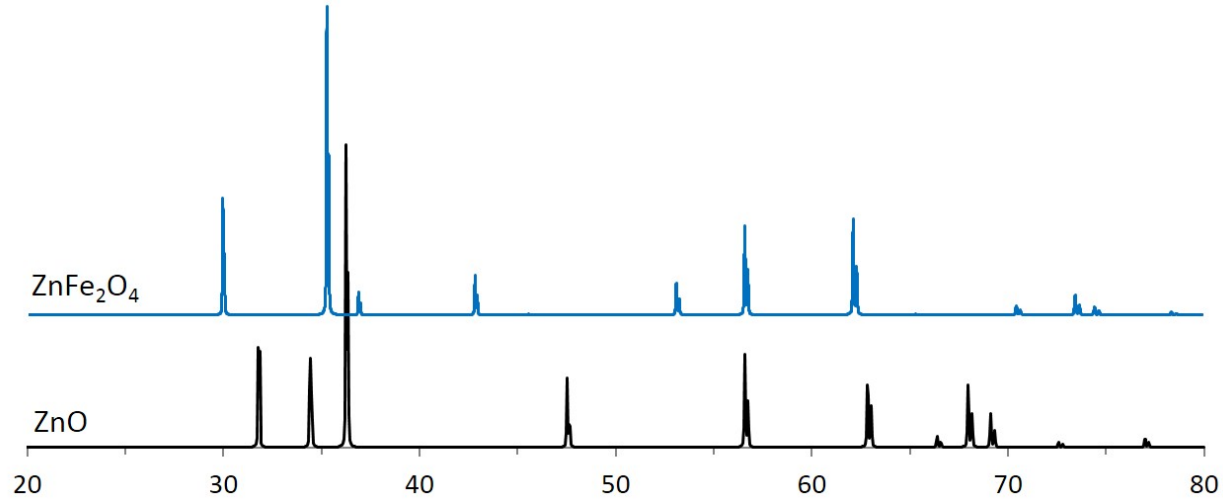

Fig. S8 Simulated XRD patterns using a 1.54056 Å radiation (Cu Kα) of the wurtzite ZnO crystal and the spinel $ZnFe_2O_4$.

Using the DFT with LSDA+U scheme, it produces the bandgap of 1.95 eV, which agrees well with the well-known bandgap 1.92 eV for the spinel structure. The bandgap of inverse spinel structure was calculated to be 2.14 eV.

Section 3. Additional figure

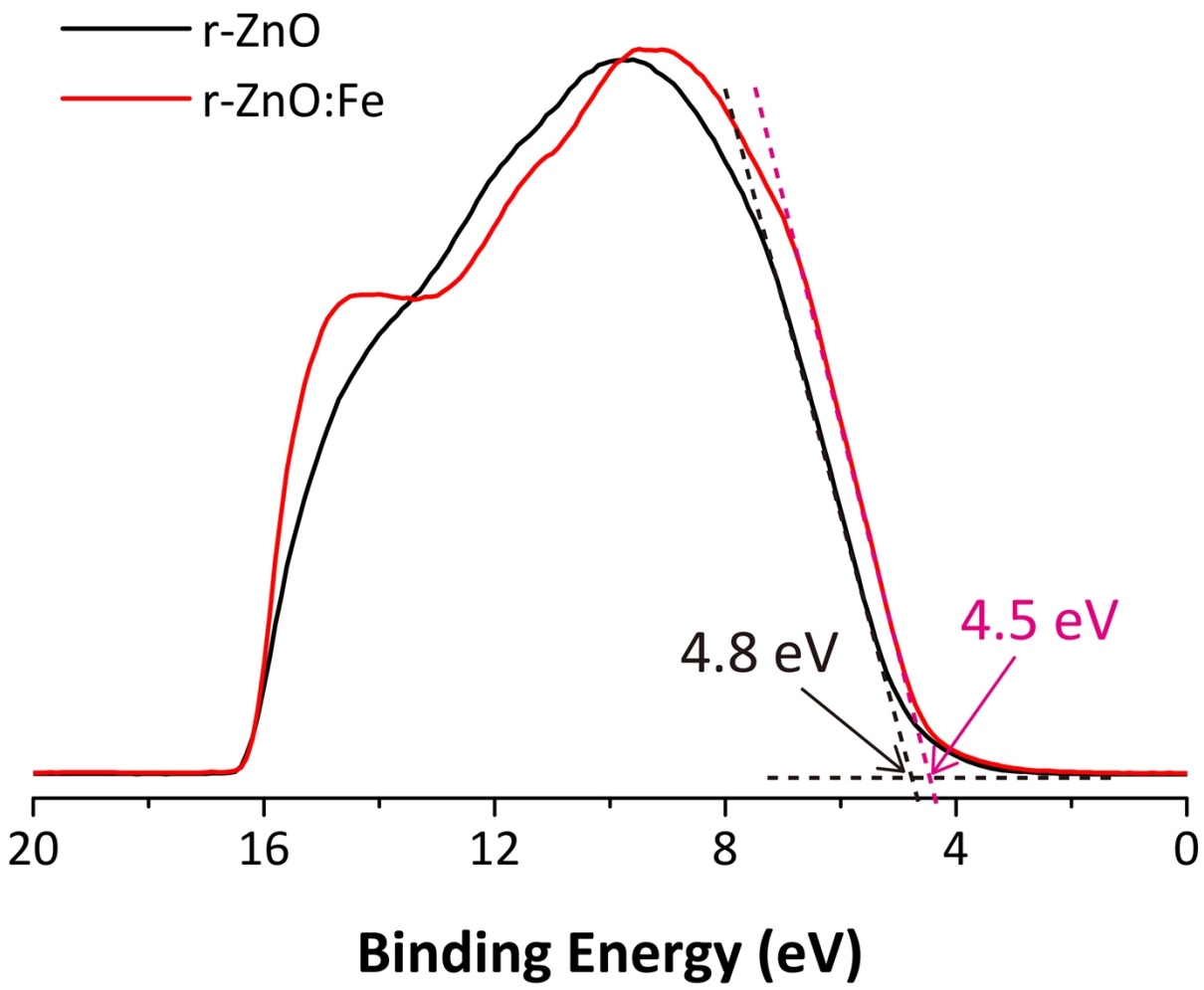

Fig. S9 The UPS spectra of r-ZnO and r-ZnO:Fe

References

[1] G. Kresse and J. Furthmüller, Phys. Rev. B **54**, 11169 (1996).

[2] P. E. Blöchl, Phys. Rev. B **50**, 17953 (1994).

[3] G. Kresse and D. Joubert, Phys. Rev. B **59**, 1758 (1999).

[4] S. L. Dudarev, G. A. Botton, S. Y. Savrasov, C. J. Humphreys, and A. P. Sutton, Phys. Rev. B **57**, 1505 (1998).

5] J. P. Perdew, K. Burke, and M. Ernzerhof, Phys. Rev. Lett. 77, 3865 (1996).

[6] S. Lany and A. Zunger, Phys. Rev. B **72**, 035215 (2005).

[7] A. Janotti and C. G. Van de Walle, Appl. Phys. Lett. **87**, 122102 (2005).

[8] R. Blachnik, J. Chu, R. R. Galazka, J. Geurts, J. Gutowski, B. Hönerlage, D. Hofmann, J. Kossut, R. Lévy, P. Michler, U. Neukirch, T. Story, D. Strauch, and A. Waag, *Landolt-Börnstein: Numerical Data and Functional Relationships in Science and Technology, New Series*, Vol. III/41B _Springer, Heidelberg, 1999.

[9] P. Erhart, K. Albe, and A. Klein, Phys. Rev. B **73**, 205203 (2006).

[10] G. Zwicker and K. Jacobi, Solid State Commun. **54**, 701 (1985).

[11] R. T. Girard, O. Tjernberg, G. Chiaia, S. Söderholm, U. O. Karlsson, C. Wigren, H. Nylén, and I. Lindau, Surf. Sci. **373**, 409 (1997).

[12] Debjani Karmakar1, S. K. Mandal, R. M. Kadam3, P. L. Paulose, A. K. Rajarajan, T. K. Nath, A. K. Das, I. Dasgupta, and G. P. Das. Phys. Rev. B 75, 144404 (2007).

[13] F. Ahmed , S. Kumar , N. Arshi , M. S. Anwar and B.H. Koo, Cryst.Eng.Comm. 14, 4016 (2012).